International Journal of Nanomedicine

Dovepress

open access to scientific and medical research

Open Access Full Text Article

ORIGINAL RESEARCH

Polyvinyl Alcohol Capped Silver Nanostructures for Fortified Apoptotic Potential Against Human Laryngeal Carcinoma Cells Hep-2 Using Extremely-Low Frequency Electromagnetic Field

Hany G Attia[1], Mai Abdelhalim Hamouda[2], Saeed Alasmari[3], Dalia F El-Telbany[4], Zaenah Zuhair Alamri[5], Safa H Qahl[5], Mohammad Y Alfaifi[6], Majid Mohammad Al-Sawahli[7], Sara Abd El Wahed[8]

[1]Department of Pharmacognosy, College of Pharmacy, Najran University, Najran, Saudi Arabia; [2]Department of Oral Pathology, Faculty of Dentistry, King Salman International University, El-Tur, Egypt; [3]Department of Biology, College of Science and Arts, Najran University, Najran 1988, Saudi Arabia; [4]Department of Pharmaceutics, Faculty of Pharmacy, Modern University for Technology and Information (MTI), Cairo, Egypt; [5]Department of Biological Science, College of Science, University of Jeddah, Jeddah, Saudi Arabia; [6]Department of Biology, College of Science, King Khalid University, Abha, Saudi Arabia; [7]Department of Pharmaceutics, College of Pharmacy, The Islamic University, Najaf, Iraq; [8]Department of Oral Pathology, Faculty of Dentistry, The British University in Egypt, Cairo, Egypt

Correspondence: Majid Mohammad Al-Sawahli, Department of Pharmaceutics, College of Pharmacy, The Islamic University, Najaf, Iraq, Tel +201119925299, Email majidalsawahli@gmail.com; Hany G Attia, Department of Pharmacognosy, College of Pharmacy, Najran University, Najran, Saudi Arabia, Tel +966555857605, Email hgattia@nu.edu.sa

Purpose: : Polyvinyl alcohol-capped silver nanostructures (cAgNSs) were investigated in order to enhance the cytotoxicity, pro-apoptotic, and oxidant patterns of in human laryngeal carcinoma Hep-2 cells by employing a 50 mT electromagnetic field (LEMF) for 30 min.

Methods: Wet chemical reduction was used to synthesize the cAgNSs, and after they had been capped with polyvinyl alcohol, they were specifically examined for particle size analysis and structural morphology. To visualize how the silver may attach to the protein targets, a molecular docking study was conducted. Estimation of cytotoxicity, cell cycle progression supported by mRNA expression of three apoptotic-promoting genes and one apoptotic-resisting.

Results: Particle size analysis results were a mean particle size of 157.3±0.5 nm, zeta potential value of −29.6 mV±1.5 mV, and polydispersity index of 0.31±0.05. Significantly reduction of IC_{50} against Hep-2 cells by around 6-fold was concluded. Also, we obtained suppression of the proliferation of Hep-2 cells, especially in the G_0/G_1 and S phases. Significant enhanced mRNA expression revealed enhanced induced CASP3, p53, and Beclin-1 mediated pro-apoptosis and induced NF-κB mediated autophagy in Hep-2 cells. Augmented levels of GR, ROS and MDA as oxidative stress biomarkers were also obtained. HE staining of Hep-2 cells exposed to cAgNSs and LEMF confirmed the enhanced apoptotic potential comparatively.

Conclusion: By conclusion, the developed nano-sized structures with the aid of extremely-low frequency electromagnetic field were successful to fortify the anti-cancer profile of cAgNSs in Hep-2 cells.

Keywords: electromagnetic field, silver nanoparticles, apoptosis, laryngeal carcinoma

Introduction

As the second most common respiratory cancer and the second most common head and neck cancer, laryngeal carcinoma is a frequent and significant reason of morbidity and mortality.[1,2] In the United States, laryngeal cancer is anticipated to cause 13,150 new cases and 3710 fatalities in 2018.[1] 0.8% of new cases of cancer and 0.6% of all cancer-related fatalities are caused by laryngeal cancer, respectively.[3,4] Targeted drugs are currently being developed as an additional option to address problems caused by conventional therapies like surgery, radiotherapy, and chemotherapy.[5] The development of

Received: 23 January 2024
Accepted: 22 June 2024
Published: 10 September 2024

Graphical Abstract

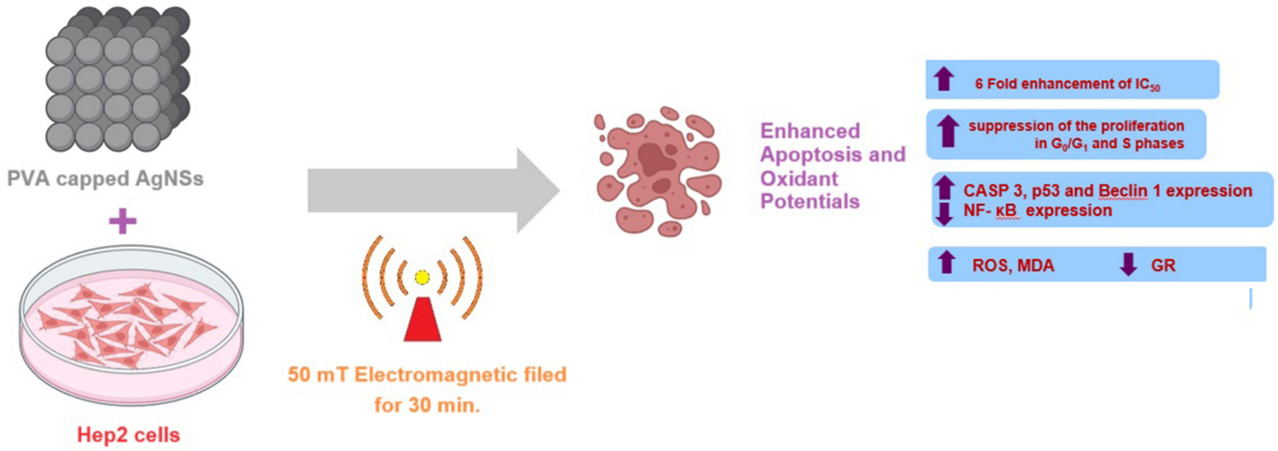

novel drug nanocarriers, personalized anticancer medications, and methods for targeted delivery of therapeutic antibodies are a few examples of how science has accelerated efforts to augment targeting of drug and minimize undesirable adverse consequences.[6]

Due to the superior physicochemical characteristics of materials at the nanoscale, cancer nanomedicine has lately concentrated on nanotechnology technologies to develop novel nanodrugs for cancer therapy.[7] It has been revealed that the cytotoxicity of metallic nanoparticles is 9 times higher in cancer cells than in normal cells, which is sufficient evidence of the particles' ability to poison and kill cancer cells in the context of cancer treatment.[8]

Numerous papers have explored the intrinsic anti-inflammatory, antibacterial, antiviral, and antifungal actions of silver. This is due to the possible toxicity, distinctive physiochemical characteristics, and biofunctional behaviors of nanosilver-based materials. Of all the nanostructures developed utilizing nanotechnology, silver nanostructures (AgNSs) have received the greatest research and exploration.[9] AgNSs have high promise as an anticancer drug, according to recent investigations.[10] According to several studies, AgNSs can kill cancer cells by a number of different mechanisms, such as oxidative stress, DNA damage, cell cycle arrest, apoptosis, and necrosis.[11–14] AgNSs are also effective radiation and chemotherapy sensitizers[15] and radiotherapy[16,17] and they have strong anticancer activity in a number of animal models.[18–20] Silver shows minimal toxicity but limited absorption because of the human body's efficient physiological detoxification system. AgNSs are a practical way to get around this problem. In fact, by internalizing AgNSs through endocytosis and other absorption mechanisms, cells may release Ag+ ions, a reactive species of silver, at the desired places.[21]

Because electromagnetic fields have impacts on living things that initiate, speed up, or stop biological processes,[22] their application for therapeutic purposes has grown. The use of therapeutic electromagnetic fields, in particular the extremely-low frequency electromagnetic field (LEMF), has been proposed for the treatment of cancer since it was found that magnetic waves interfere with many biological processes. Extremely low-frequency electromagnetic fields are defined as having frequencies below 300 Hz. Because of their low energy, these electromagnetic fields do not directly damage DNA because they do not break molecular bonds. The effects of LEMF on cells and tissues are also non-thermal, non-invasive, and non-ionizing.[23] These characteristics have sparked research on how LEMF affects the start of many illnesses, including cancer. Despite the fact that certain studies relate exposure to LEMFs to the development of cancer,[23–25] other studies employing human tumors and experimental models have shown that LEMF does not increase the chance of acquiring a variety of tumor forms, including liver cancer.[26–28] The LEMF therapy with tumor-specific frequencies is feasible, well-tolerated, and may show positive biological benefit in patients with advanced malignancies.[26–28] More study on the impact of LEMFs on cancer cells is necessary since the existing data are not

adequate to show that LEMFs suppress carcinogenesis. This study's objective was to comparatively examine the improvement of cytotoxicity, proapoptotic profile and oxidant potential associated to polyvinyl alcohol-capped silver nanostructures against laryngeal cancer cell line Hep-2 utilizing low frequency magnetic field.

Materials and Methods

Materials and Cell Lines

The solution of silver nitrate (AgNO3; CAS number: 9002-89-5) was provided by Merk (Darmstadt, Hessen, Germany). Sigma-Aldrich (St. Louis, MO, USA) provided the polyvinyl alcohol (PVA; CAS number: 9002-89-5), 99% sodium borohydride (NaBH4; CAS number: 16940-66-2), and ethanol (CAS number: 64-17-5). The chemicals and solvents used were all of analytical grade.

Hep-2 cells were kindly supplied from the Holding company, Tissue Culture Department, for production of vaccines, sera, and drugs (VACSERA, Giza, Egypt). Cells were kept alive in MEM-E media supplemented with 10% fetal bovine serum at 37°C (Jouan SA, Saint-herblain, Pays de la Loire, France) in a humidified environment of 5% CO_2. Cells were maintained according to manufacturing protocol where the growth medium was decanted and cells were washed with phosphate buffer saline (Adwia Pharmaceuticals, El Sharkeya, Egypt). 0.25% trypsin and 0.05% (v/v) EDTA (GIBCO) were added to the cells for 5 minutes at 37°C. Depending on the situation, detached cells were splatted.

Formulation of Capped Silver Nanostructures (cAgNSs)

Wet chemical reduction was used to fabricate silver nanostructures, with 99% NaBH4 serving as a reducing agent. For the formulation of PVA capped AgNSs (cAgNSs), PVA was utilized as a capping agent. In a nutshell, 800 rpm continuous stirring was utilized to mix 1 mL of 100 mM AgNO3 solution with 8.0 mL of 1% w/v PVA aqueous solution. The resultant dispersion of AgNO3 and PVA received one milliliter of a freshly made 15 mM NaBH4 aqueous solution. After another 30 minutes of stirring, a yellow tint appeared, signifying the development of AgNSs. After centrifuging the precipitate, it was cleaned with ethanol/water (90:10 v/v) and lyophilized.

The synthesized cAgNSs were resuspended in deionized water at a starting concentration of 100 μM/mL to evaluate the cytotoxicity of the prepared particles on Vero cells.

Characterization of cAgNSs

Particle Size Analysis

For the examination of cAgNSs average particle sizes, zeta potential and Polydispersity index (PDI), Malvern Instruments-UK's Zetasizer Nano-ZS laser diffraction method was used. Deionized water was used to dilute one milliliter of the sample in a disposable cuvette.

Nanostructures Morphology

Field emission scanning electron microscopy (FESEM) (JSM-7600F, Joel-Japan) was used to investigate nanostructures surface morphology of cAgNSs.

Molecular Docking

In a molecular modeling research, the Molecular Operating Environment (MOE), a software platform for drug discovery, integrates visualization, modeling, simulations, and technique development. Molecular Operating Environment (MOE, 2019) software was used to conduct molecular modeling experiments using a Dell Core i7 computer with 1.9 GHz, 16 GB of RAM, and Windows 10 64-bit operating system. With an RMSD (root mean square deviation) gradient of 0.05 kcal/mol and the MMFF94X force field utilizing MOE, energy minimizations were carried out. Partial charges were also automatically computed. From Protein Data Bank, which can be viewed at https://www.rcsb.org/pdb, the crystal structure of the human laryngeal carcinoma cell line Hep-2 was accessed on December 30, 2020.

Preparation of Target Protein (6YHL) for Docking

1- Removing the water molecules from the protein's active site.

2- Addition of hydrogen atoms with their typical geometries to the structure.

3- The MOE site finder generated the active binding sites to create the dummy sites as the binding pocket.

4- The obtained pocket was saved as Moe to be used in predicting the ligand-protein

Using the MMFF94 force field, the native ligand was minimized to its lowest energy. Following 3D protonation and the rectification procedure, the final form was produced. The ligand (Polyvinyl alcohol-silver nitrate) was positioned in the site using the triangle matcher approach after the general docking scenario was run for 100 ns on the stiff receptor atoms. The GBVI/WSA dG procedures for rescoring were used, along with the London dG as a scoring function. The binding free energy (S, kcal/mol) and hydrogen bonds between substance and protein-containing amino acids with lengths under 3.5 A were used to rank the top five poses. Additionally, the results pose-with-pose in the co-crystal ligand position and before and after amendment, respectively, were compared using the RMSD and RMSD-refine fields.

Cytotoxicity Assay

The synthesized cAgNSs were resuspended in deionized water with a starting concentration of 100 M/mL in order to evaluate the cytotoxicity of the manufactured nanostructure on Vero cells. According to,[29] Hep-2 cells were put to 96-well plates (TPP, Switzerland) at a density of around 2×10^3 cells per well to conduct MTT experiment to determine the antiproliferative activity. Wells were subjected to a variety of concentrations of cAgNSs and cAgNSs exposed to 50 mT LEMF for 30 min. (cAgNSs-LEMF) for 48 hours at 37°C in a carbon dioxide incubator.

Cell Cycle Progression Analysis

cAgNSs, cAgNSs-LEMF and doxorubicin as a positive control IC_{50} values were pre-calculated and delivered to Hep-2 cells (5×10^3 MCF-7 cells/well) for 48 hours. After being trypsinized, the cells were then fixed in ice-cold 60% ethanol at 40 °C and then washed once more in PBS (phosphate buffered saline). The cells were resuspended in 500 µL of Cell Signaling Technology's (CST) propidium iodide (PI) with RNase staining buffer, and incubated for 15 minutes. The data from 10,000 cells and the distribution of cell cycle phases for each sample were then evaluated using FACS analysis on a Cytek® Northern Lights 2000 spectral flow cytometer (Cytek Biosciences) using SpectroFloTM Software version 2.2.0.3 (Cytek Biosciences), USA.[30]

Annexin-V Assay

For assessing of apoptosis, Hep-2 cells treated with cAgNSs, cAgNSs-LEMF and doxorubicin as a positive control for 48 hr and then trypsinized and washed twice with PBS. Apoptosis assessment was done via the Annexin V-FITC/PI Apoptosis Detection Kit, Cell Signaling Technology (CST), as stated by the manufacturer. In Brief, cells were resuspended in 5 µL of Annexin V-FITC and 5µL of PI (staining solution) were added then 0.5 mL of binding buffer with gentle mixing for 15 minutes at room temperature in dark place. The cells were then subjected to a FACS analysis utilizing a Cytek Biosciences Northern Lights 2000 spectral flow cytometer and SpectroFloTM Software version 2.2.0.3 (Cytek Biosciences), USA.[31]

mRNA Expression of Apoptosis-Related Genes by Quantitative Real-Time Polymerase Chain Reaction (RT-PCR)

The identical chemicals and kits were used to perform this test according to[32,33]'s reports. Table 1 gives the primer sequences for CASP3, p53, Beclin-1 and NF-kB. Results were validated using the relative quantification method. Utilizing the relative quantification (ΔΔCt) approach, results were verified. The runs mean was normalized with the GAPDH mean, and the gene expression was calculated in triplicates.

Oxidative Stress

Glutathione Reductase Enzyme Assay

The glutathione reductase enzyme (GR), one of the markers of oxidative stress, was measured for the groups of cAgNSs and cAgNSs-LEMF using commercial kits (ABCAM, Cambridge, UK). A microplate-reader technique was employed to

Table 1 Primer Sequences Used for RT-PCR

Primer		Sequence
CASP3	Forward primer	5- CTCGGTCTGGTACAGATGTCGA-3'
	Reverse primer	5- CATGGCTCAGAAGCACACAAAC-3'
p53	Forward primer	5'-TCA GAT CCT AGCGTC GAG CCC-3'
	Reverse primer	5'-GGG TGT GGA ATC AACCCA CAG-3'
Beclin-1	Forward primer	5'-CTGGACACTCAGCTCAACGTCA-3'
	Reverse primer	5'-CTCTAGTGCCAGCTCCTTTAGC-3'
NF-kB	Forward primer	5'-GCAGCACTACTTCTTGACCACC-3'
	Reverse primer	5'- TCTGCTCCTGAGCATTGACGTC-3'
GAPDH	Forward primer	5'- GTCTCCTCTGACTTCAACAGCG-3'
	Reverse primer	5'- ACCACCCTGTTGCTGTAGCCAA-3'

calculate the intracellular GR activity. Hep-2 cells were infused into 6-well plates at a density of 1×10^6 cells/mL, and then exposed to the formulation's IC_{50} value for 48 hours. After that, cells were taken out and cleaned with PBS. The Bradford technique (Sangon, Shanghai, China) was used to measure the absorbance of a cell extract at 412 nm in order to determine the GR concentration.

Reactive Oxygen Species Assay (ROS) and Malondialdehyde (MDA) Assays

$5x10^3$ Hep-2 cells/well in 96-well plates were produced and treated for 24 hours with IC_{50} concentrations of cAgNSs, and cAgNSs-LEMF. Samples were analyzed in contrast to the control group of untreated cells. Cell staining was carried out for 45 minutes using a commercial kit (ABCAM, Cambridge, UK) and 10 M 2.7-dichlorofluorescein diacetate. Using the BioVision Lipid Peroxidation Assay Kit from BioVision Incorporated, Milpitas, California, USA, MDA levels in cells were also assessed.

Hematoxylin and Eosin Staining of Hep-2 Cells

On three clean slides for each treatment, 50 microliters of cAgNSs, cAgNSs-LEMF were applied. After being air dried, methanol fixed, and rehydrated in progressive alcohol concentrations (100%, 90%, 75%, and 50%), slides were processed. Slides were cleaned for five minutes with distilled water. The slides were twice rinsed with distilled water after being submerged in filtered hematoxylin (HE) stain for three minutes. Slides were washed with distilled water after spending 5 seconds in filtered eosin stain. After drying, slides were placed in xylene, mounted with Canada balsam, wrapped with coverslips, and let to air dry. A 400-power photomicrograph was taken of each slide in 10 small fields. A digital camera (Canon, Japan) placed on a light microscope was used for this. The computer system received the images for analysis. Fields were selected based on the presence of the most apoptotic cells. The presence of apoptosis morphological criteria was determined by judging the photomicrographs subjectively.

Statistical Analysis

The study's results were displayed using the averages and standard deviations (SD) of at least three different runs. To compare statistical data between treatments, Tukey's test or a one-way analysis of variance were utilized (the two-tailed p value threshold for significance was 0.05). The program used was IBM SPSS software (SPSS Inc., Chicago, IL, USA).

Results and Discussions

The utilization of LEMF in cancer therapy is gaining popularity. Evidence of therapeutic characteristics includes a marked decrease in the development of several tumors, including hepatocellular, gastrointestinal, sarcoma, and breast cancers.[34–37] LEMF may also relieve general symptoms and increase survival for individuals with advanced cancer.[38,39]

Formulation and Characterization of cAgNSs

In the present study, cAgNSs were synthesized using PVA as capping agent. UV-visible spectrum displayed the absorbance maxima (λ_{max}) of silver colloid at 420 nm confirming the reduction of silver in less symmetric spectrum (Figure 1). Additionally, the average particle size of cAgNSs determined by dynamic light scattering (DLS) study was 157.3 0.5 nm, which showed promise for enhancing absorption and residence duration inside biological systems.[29] Interestingly, Zeta potential of the prepared cAgNSs obtained a negative value of −29.6 mV±1.5 mV that indicated strong electrostatic attraction between the silver ions and the surrounding metabolites which assure satisfied stability, as the surface charge retards aggregation of formed nanostructures.[40] It was determined that stable nanostructures have been defined as those with a zeta potential of >+25 mV or 25 mV.[41] Also, cAgNSs is dispersed with an average PDI of 0.31 ±0.05 reflecting moderate particle size distribution.[42]

FESEM imaging was used to determine the morphological structure of the synthesized nanostructures, and the results revealed irregularly shaped, discrete with little agglomeration and exhibiting smooth surfaces free of holes or fissures (Figure 2).

Molecular Docking

Molecular docking is a method for determining how one molecule will prefer to interact with another when they are joined to create a stable complex. In order to estimate the affinity and activity of the small molecule, docking can be utilized to forecast how drug candidates will attach to their protein targets. Therefore, in the present investigation, we applied molecular docking to cAgNSs to illustrate anticancer activity evaluation in vitro against human laryngeal carcinoma cell line Hep-2 (PDB:6YHL). The obtained results of docking scores and energies are totally presented in (Table 2) showing a good binding score of −5.6342 kcal/mol by the hydrogen accepting ability of one of the oxygen atoms of the nitro group (O 22) towards TYR 206 amino acid residues with hydrogen bond 3.35Å and energy

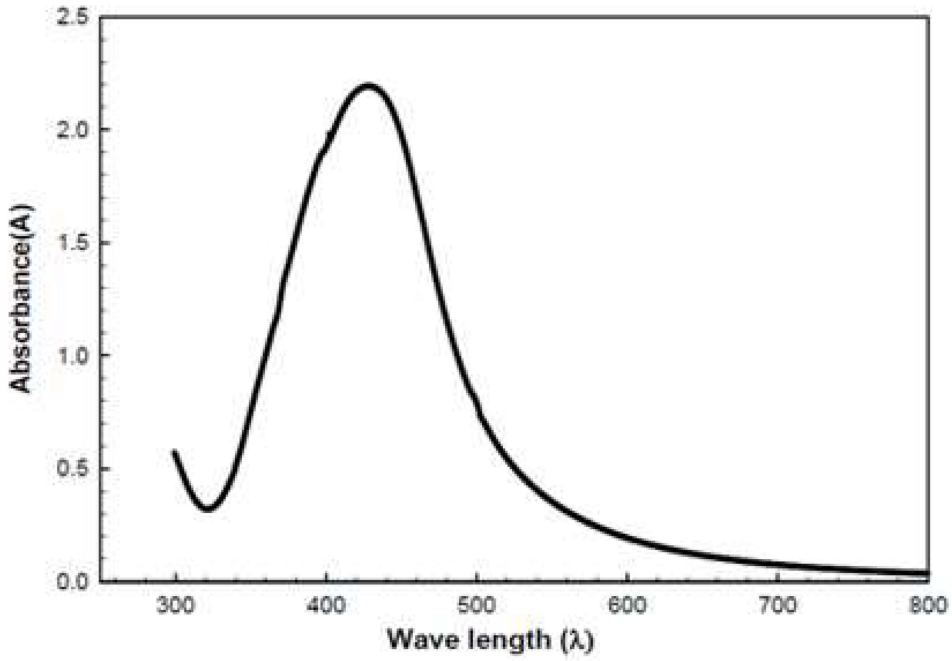

Figure 1 UV-visible spectrum of cAgNSs.

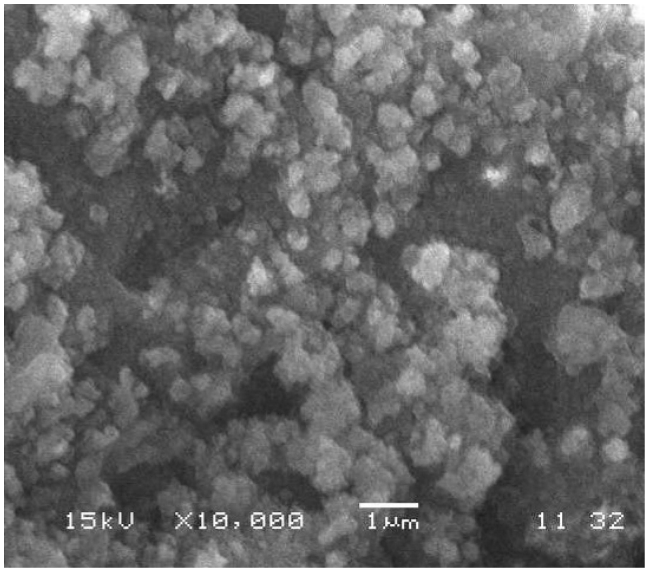

Figure 2 FESEM image of cAgNSs.

stabilization by −0.6 kcal. In addition to two metal bonds between the Ag atom and GLU 639 amino acid residues. The interactions between almost all atoms in the ligand (cAgNSs) and amino acid residues of 6YHL were recorded in (Table 3). The RMSD value was determined to be 0.94Å proving that the examined inhibitor responds well to our docking approach. The best possible conformation of Pva-NO_3 inside the protein central activity is shown in Figure 3. The best-docked conformation is the one that has the lowest binding energy and the maximum affinity. Because the docking program (MOE) was able to replicate experimentally observed binding modes, as in this finding, it identifies the specific target-ligand conformation, analysis of this docked ligand with the chosen protein also brought into focus a very important molecular interaction. In Figure 4, the interaction between cAgNSs and the active regions of the 6YHL protein was shown in a 2D image.

Table 2 Docking Scores and Energies of cAgNSs with Human Laryngeal Carcinoma Cell Line Hep-2 (PDB Code: 6YHL)

Mol	S	RMSD_refine	E_conf	E_place	E_score1	E_refine	E_score2
cAgNSs	−5.6342	0.940418	−143.132	−46.3105	−7.04985	−29.5086	−5.6342
cAgNSs	−5.61877	1.582114	−140.525	−43.7555	−7.70099	−28.4003	−5.61877
cAgNSs	−5.56809	1.714894	−143.38	−50.2424	−7.03235	−31.6837	−5.56809
cAgNSs	−5.32723	1.648978	−74.223	−43.4059	−7.37634	−29.6941	−5.32723
cAgNSs	−5.32452	1.245506	−141.233	−54.7142	−7.18993	−26.4953	−5.32452

Table 3 Interaction of cAgNSs with Human Laryngeal Carcinoma Cell Line Hep-2 (PDB Code: 6YHL)

Ligand	Receptor	Interaction	Distance	E (kcal/mol)
O 22	N TYR 206 (A)	H-acceptor	3.35	−0.6
Ag 18	OE1 GLU 639 (A)	Metal	2.71	−0.8
Ag 18	OE2 GLU 639 (A)	Metal	2.77	−3.3

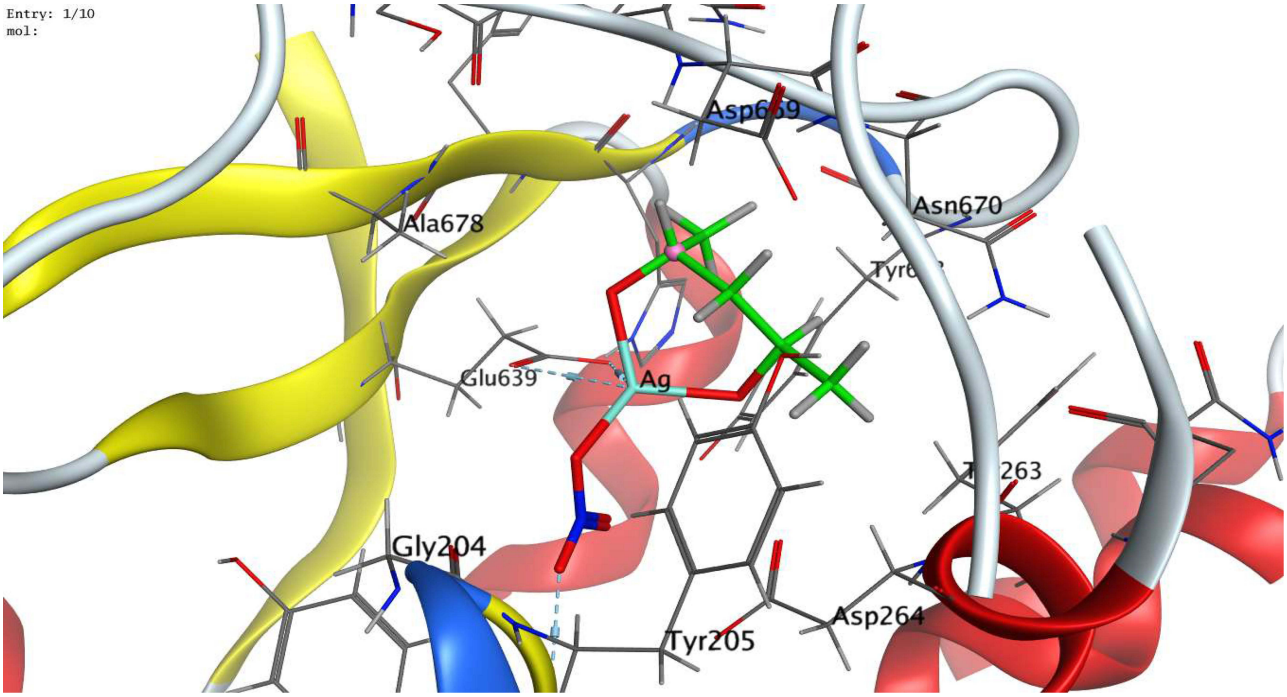

Figure 3 3D diagram shows the most likely binding conformation of cAgNSs with 6YHL and the corresponding intermolecular interactions are identified.

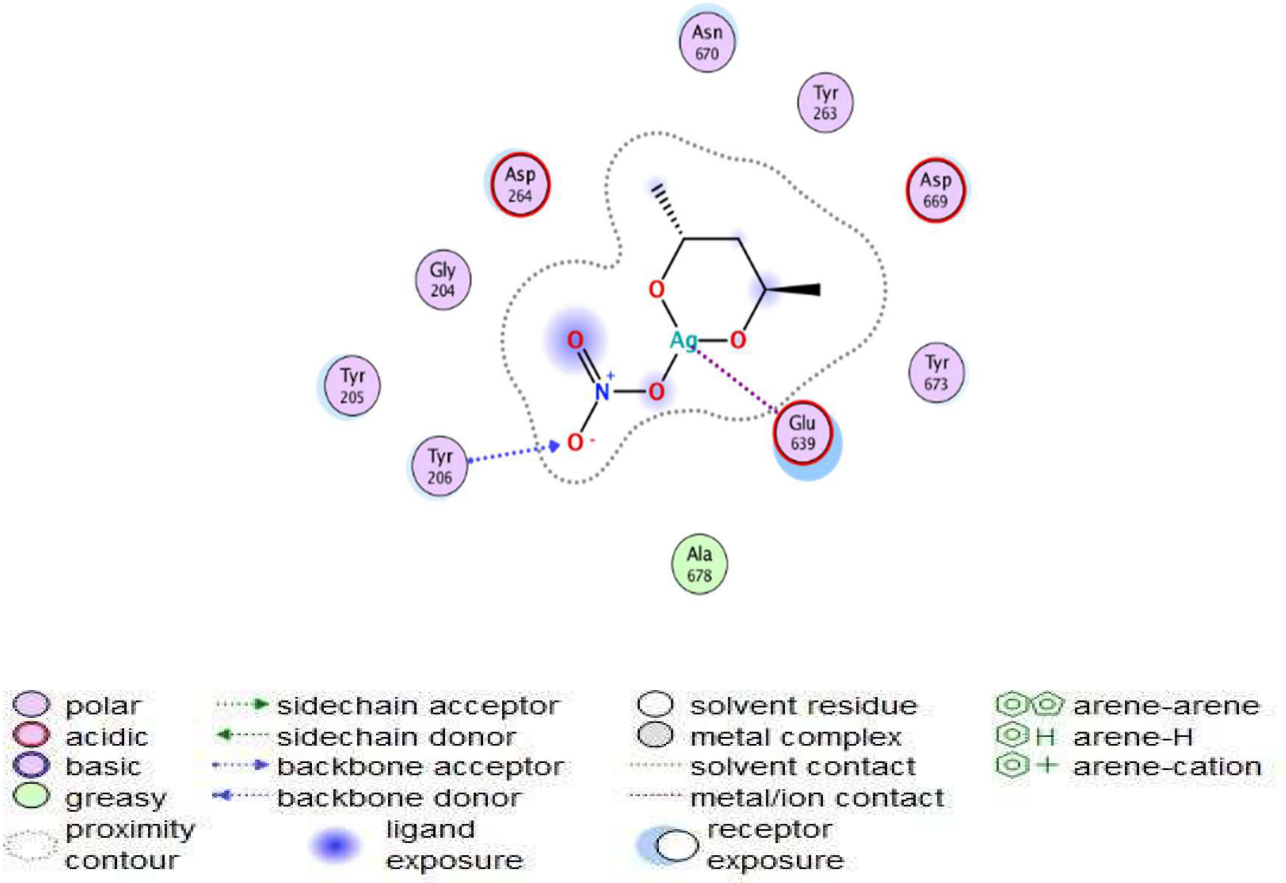

Figure 4 2D diagram shows the interaction between cAgNSs and active sites of 6YHL protein.

Cytotoxicity Assay

On Hep-2 cells, cAgNSs' antiproliferative activity was tested, and the results are depicted in Figure 5. The cAgNSs-LEMF obtained improved activity of approximately (IC_{50} = 3.29 0.4 mol/mL) compared to cAgNs (21.36 1.05 mol/mL) under the effect of magnetic induction/time values of 50 mT/15 min. The findings demonstrated that, in comparison to cAgNSs, the effect of LEMF greatly improved the cytotoxicity pattern of cAgNSs-LEMF against Hep-2 cells by around 6-fold. The observed enhanced effect of LEMF on cAgNSs cytotoxicity was consistent with other research concentrating on the use of electromagnetic fields for enhancing the cytotoxicity of silver, graphene,[43,44] and gold nanoparticles.[22] The relationship between LEMF-induced cytotoxicity and the beginning of apoptosis was determined[44] and led to the generation of ROS, which then increased sirtuin-1 (SIRT1) expression and activated p53 pro-apoptotic activity. Additionally, it was determined[43,44] that the shape of AgNSs affected the induction of electromagnetic fields around AgNSs exposed to optical stimulation of localized surface plasmon resonances.

Cell Cycle Progression Analysis

The impact of cAgNSs and cAgNSs-LEMF on the distribution of the cell cycle in Hep-2 cells was examined. Hep-2 cells were exposed to predetermined IC_{50} concentrations of cAgNSs and cAgNSs-LEMF for 48 hours. Control untreated Hep-2 cells obtained rapid growth properties, with 8.76 ± 0.76% at theG0/G1 phase, 44.31 ± 0.21% at the S phase and 46.92 ± 3.2% at the G2-M phase (Figure 6a). The DNA content of the cells was then measured using flow cytometry, following staining with propidium iodide (PI) (as depicted in Figure 6b and c). In Hep-2 cancer cells, both cAgNSs and cAgNSs-LEMF significantly increased the population of cells in the S-phase of the cell cycle. However, the percentage of cells arrested in the S-phase was higher after treatment with cAgNSs compared to cAgNSs-LEMF. Specifically, the percentage increased from 44.31% ± 0.21% (in untreated control cells) to 71.4% ± 0.9% with cAgNSs, while it increased to 68.3% ± 0.7% with cAgNSs-LEMF. A graphical presentation of each phase was displayed in Figure 6d. The observed pro-apoptotic tendency may be connected to the generation of reactive oxygen species, which then causes DNA damage and protein denaturation, finally inducing apoptosis.[45]

Annexin-V Assay

Results were displayed in Figure 7a–c to promote cell apoptosis after assessment of the proportion of cells with positive annexin-V staining in the intended groups (control, cAgNSs, and cAgNSs-LEMF) incubations. The cAgNSs-LEMF certainly enhances early, late, and total cell death greatly as compared to all other incubations. Figure 7d displays examples of each form of cell death.

The synthesized nanostructure with the LEMF pattern, cAgNSs-LEMF, obtained the highest pattern in enhancing pre-G phase, concluding apoptotic cell death, which was verified by the annexin-V staining experiment. The obtained results were consistent with[22] where it was shown that intermittent exposure of Hep-2 cells to a 25 and 50 mT of LEMF affected the cell cycle profile and was demonstrated by noticed elevated up- and down-regulation of apoptosis-related genes,

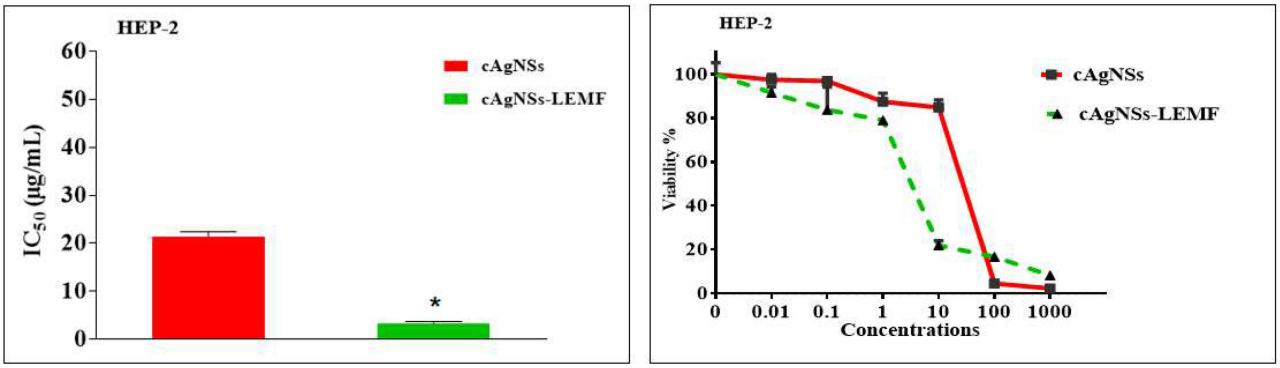

Figure 5 IC_{50} and Dose -response curves of cAgNSs and cAgNSs-LEMF in Hep-2 cells.
Notes: *Significant difference (p< 0.05) when compared to cAgNSs.

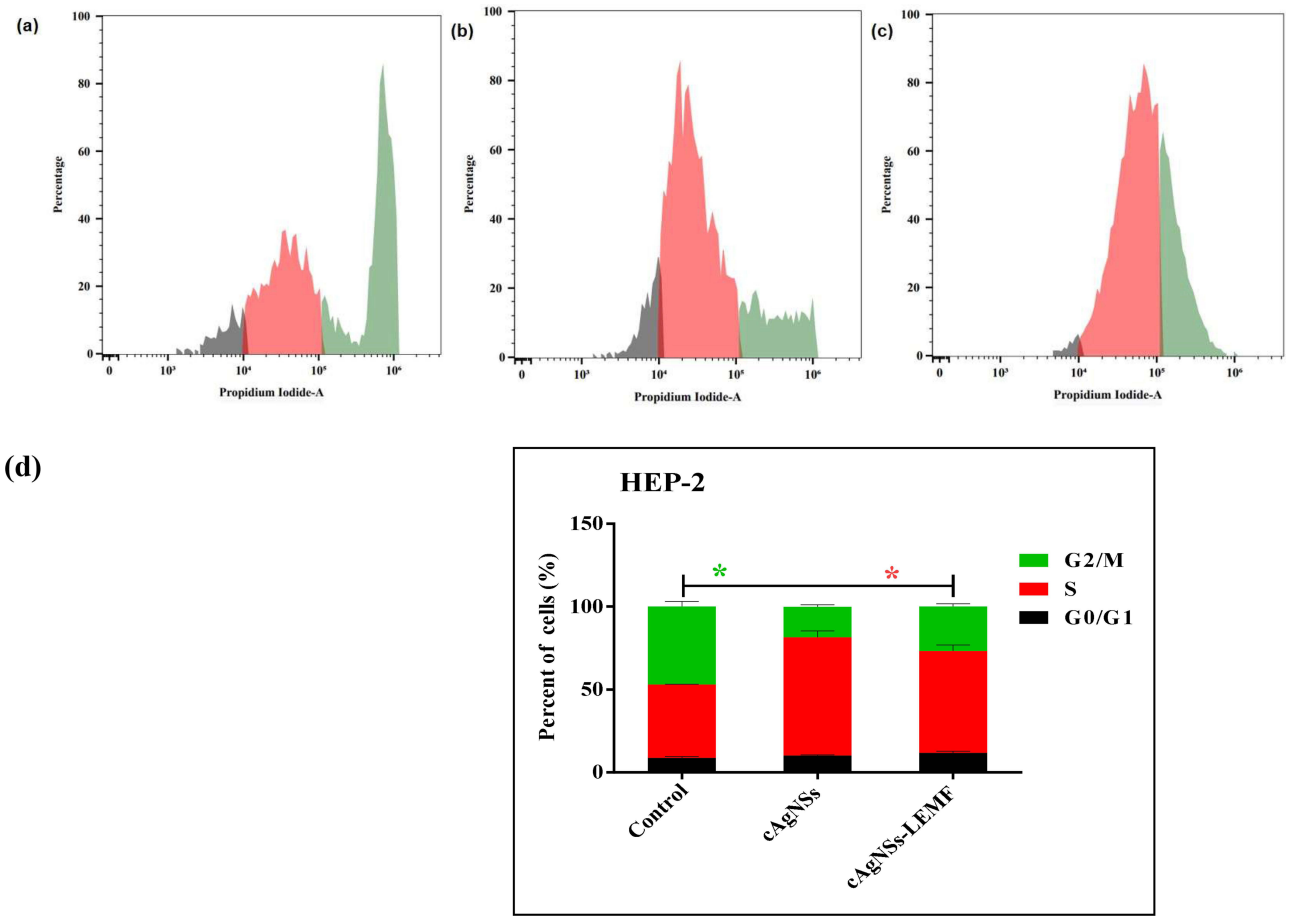

Figure 6 Impact of cAgNSs on cell cycle phases. (**a**) Control, (**b**) cAgNSs, (**c**) cAgNSs-LEMF, (**d**) Graphical presentation of each phase.
Notes: *Significant difference from control group at $p < 0.05$.

particularly due to the presence of gold nanoparticles inside the cells allowing introduction and progression of cell damage, particularly cancerous cells. Furthermore, our results supported the idea that total cell death, early and late apoptosis, and alter the pattern of LEMF to induce apoptosis in osteoclasts by increasing intracellular and nucleus Ca^{2+} concentration, which in turn increases endonuclease activity, inducing DNA fragmentation and apoptosis.[46] By acting on membrane proteins, the metallic nanoparticles utilized in LEMF can also activate signaling pathways and stop the development of cancer cells.[22]

mRNA Expression of Apoptosis-Related Genes

Figure 8 showed the statistically different ratios of the gene expression profiles of three apoptotic-promoting genes (CASP3, p53, and Beclin-1) and one apoptotic-resisting gene (NF- κB) in cells treated with cAgNSs and cAgNSs-LEMF. In comparison to control and cAgNSs, cAgNSs-LEMF produced the greatest expression of the CASP3, p53, Beclin-1, and NF- κB genes in Hep-2 cells. Under the influence of an extremely low frequency electromagnetic field, cAgNSs-LEMF improved the gene expression of the used apoptotic markers, confirming a strengthened anticancer potential associated with the synthesized silver nanostructures.

Since CASP3 activation is necessary for chemotherapeutic drug-mediated induction of apoptosis, it is possible to anticipate how responsive cancer cells will be to these medications. The fold changes for the cAgNSs and cAgNSs-LEMF groups were 3.15 and 3.24, respectively. Comparing it to an untreated positive control, cAgNSs-LEMF produced a larger level of apoptotic impact. When compared to cAgNSs, cAgNSs-LEMF showed a 1.04-fold rise in CASP3 level.

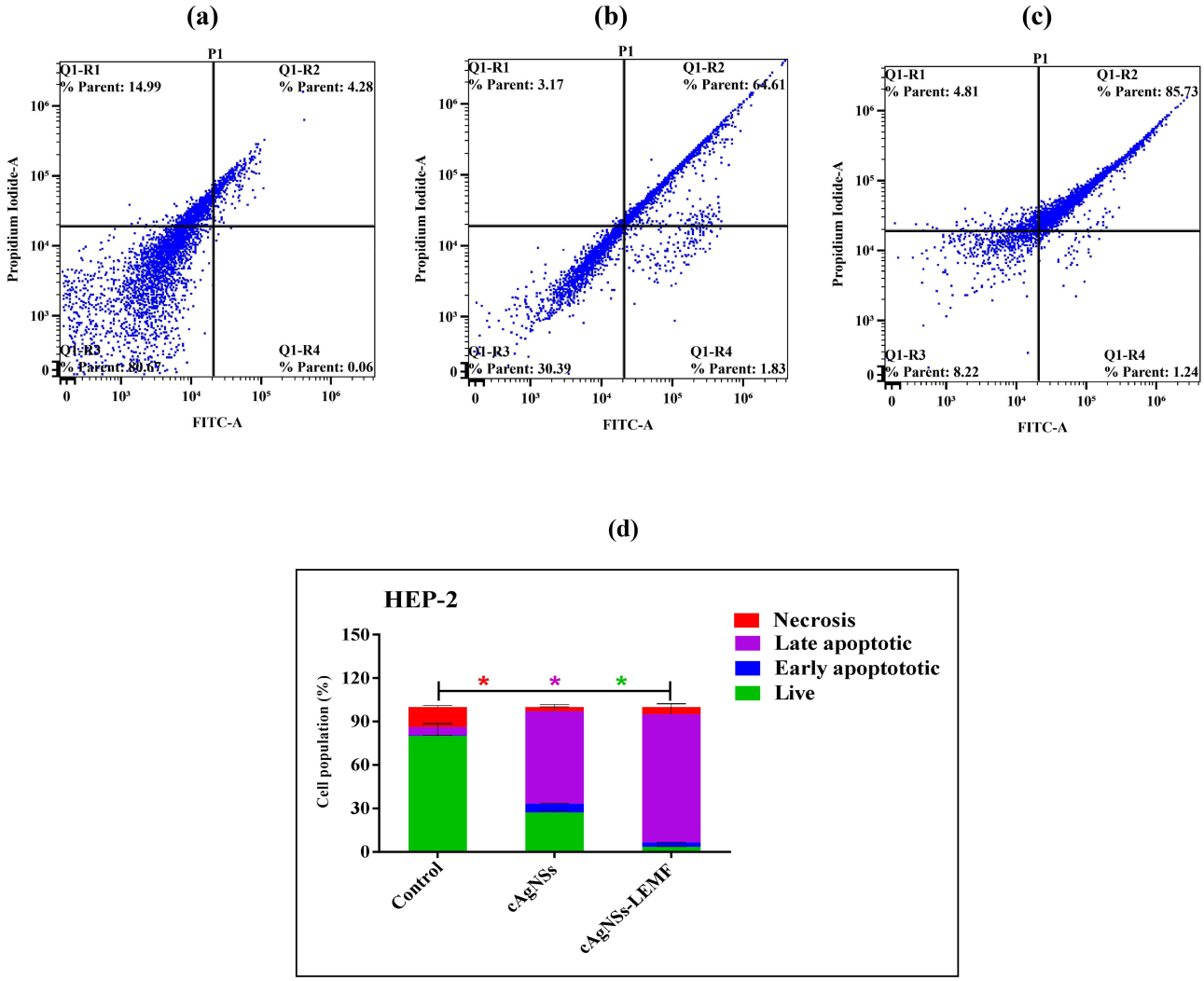

Figure 7 Impact of cAgNSs on annexin-V FITC positive staining Hep-2 cells. (**a**) Control, (**b**) cAgNSs, (**c**) cAgNSs-LEMF, (**d**) Graphical presentation of early and late apoptotic, necrotic and total cell death.
Notes: *Significant difference from corresponding control group at p < 005.

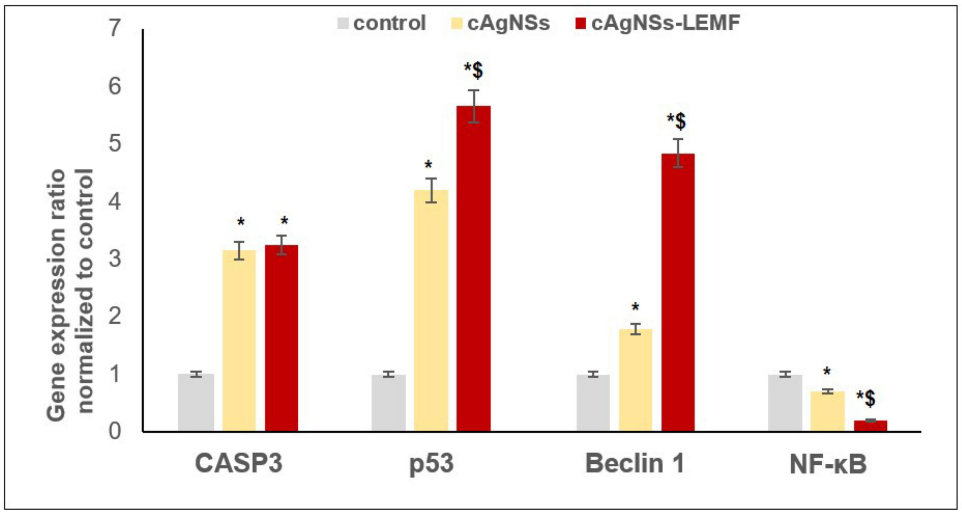

Figure 8 Impact of cAgNSs-LEMF on Caspase 3, p53, Beclin-1 and NF- κB in Hep-2 cells. Data are presented as M±SD (n=6).
Notes: *Significant difference compared to control (p < 0.05). $Significant difference compared to cAgNSs (p < 0.05).

Caspases start the apoptotic process, which is fundamentally thought of as a crucial component of treatments that target cancer.[47] The insensitivity of cancers cells to several chemotherapeutic drugs may be caused by CASP3 deficiency.[48]

According to several studies, the p53 protein is a powerful transcription factor that can cause cell cycle arrest and apoptosis to begin.[49] p53 is necessary for a variety of chemotherapy drugs to cause apoptosis. In fact, chemotherapy is typically ineffective against cancers with a defect in the p53 pathway.[50] The fold changes for both the cAgNSs and cAgNSs-LEMF groups were 4.1 and 5.66, respectively. Comparing cAgNSs-LEMF to cAgNSs, apoptotic activity was greater in the cAgNSs-LEMF. When compared to cAgNSs, p53 expression was 1.38 times higher in cAgNSs-LEMF.

A key biomarker of autophagy is Beclin-1. Beclin-1 stimulates LC3-I's lipidation to produce LC3-II, which localizes to the autophagosome membrane to activate the development of autophagosomes.[51] The fold changes for both the cAgNSs and cAgNSs-LEMF groups were 1.79 and 4.85, respectively. Comparing cAgNSs-LEMF to cAgNSs, autophagy profile was greater in the cAgNSs-LEMF. When compared to cAgNSs, Beclin-1 expression was 2.71 times higher in cAgNSs-LEMF.

A transcription factor known as nuclear factor kappa-light-chain-enhancer of activated B cells (NF-B) has lately received extensive attention for playing a crucial role in human cancer.[52] It controls autophagy and has a vital role in regulating apoptosis.[53] It is interesting to note that a recent study found that inhibiting the mTOR pathway can positively control NF-B activity and that autophagy-related signaling affects NF-B activity.[54] Since NF-B controls Bcl-2 levels and Bcl-2 regulates autophagy by interacting with Beclin-1, modulating the balance of Beclin-1/Bcl-2 is another potential method.[55] The fold changes for both the cAgNSs and cAgNSs-LEMF groups were 0.7 and 0.21, respectively. Comparing cAgNSs-LEMF to cAgNSs, autophagy profile was greater in the cAgNSs-LEMF. When compared to cAgNSs, NF- κB expression was 3.33 times higher in cAgNSs-LEMF.

Evaluation of Oxidative Stress Markers

Free radicals are known to induce DNA damage and lipid peroxidation, which together with oxidative stress are known to stimulate the development of tumors.[56] Table 4 displayed the findings of the estimate of the parameters of oxidative stress. The most effective way to raise MDA levels in Hep-2 cells, enhance ROS production, and decrease GR activity is using cAgNSs-LEMF. Particularly, as compared to control, cAgNSs and cAgNSs-LEMF substantially suppressed GR activity by 44.17% and 49.45%, respectively. This was consistent with the LEMF's alleged ability to increase the low glutathione level in osteoblasts,[57] brain cells,[58] and neuroblastoma cells.[59]

Oxidative DNA adducts can be created when ROS and DNA bases interact. These adducts have been connected to mutagenesis and carcinogenesis.[60] Due to its crucial function, ROS play in both healthy and pathological circumstances in triggering apoptosis. According to reports, LEMF may boost ROS levels, which then activate the apoptotic pathway.[61,62] DCFH-DA was used to measure ROS production in Hep-2 cells, and ETD-SDZN NSs had the strongest green fluorescence. High quantities of ROS may impair cellular physiological function by damaging DNA, proteins, phospholipids, and other macromolecules. When ROS levels are low, the redox-sensitive MAPK, PI3K, and mTOR pathways, as well as the mTOR pathway, may be triggered by ROS in the reverse manner.[63] In rat fibroblasts, exposure to 50 Hz ELF-EMF for 3 or 24 hours has been shown to enhance ROS generation and DNA damage.[64] To better understand the biological impacts of ELF-EMF, it is necessary to further research the mechanism by which exposure to ELF-EMF alters intracellular ROS levels.[63]

Also, cAgNSs and cAgNSs-LEMF groups significantly decrease MDA levels by 27% and 40% as compared to control values, respectively. This attenuation of rise in MDA levels was evidence for inhibition of lipid peroxidation.

Table 4 Effect of cAgNSs, and cAgNSs-LEMF on Oxidative Stress Parameters

	Control	cAgNSs	cAgNSs-LEMF
GR (μU/10^6 cells)	2.443±0.15	1.364*±0.07	1.235*±0.11
ROS (Pg/10^6 cells)	54.25±7.85	209.7*±9.48	287.5*#±4.52
MDA (nmol/10^6 cells)	8.092*#±0.141	9.897*±0.028	11.55±0.067

Notes: Data are presented as mean ± SD (n = 6). *Significant difference from control group at $p < 0.05$, #significant difference from cAgNSs group at $p < 0.05$.

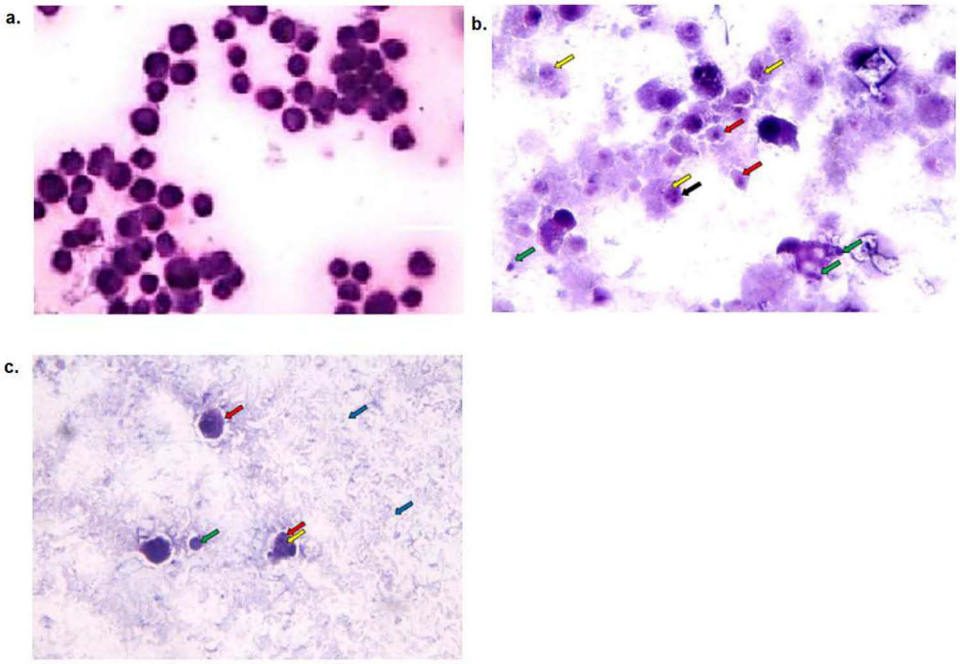

Figure 9 Hep-2 cells Microphotographs after cAgNSs, LEMF and cAgNSs-LEMF treatments. (**a**) Control, untreated Hep-2 cells exhibited regular tumor cells, nuclear pleomorphism and cellular pleomorphism. (**b**) cAgNSs, Hep-2 cells showing apoptotic cells after treatment with cAgNSs. Cells show cellular and nuclear shrinkage (red arrows), irregular cell membrane (black arrow), nuclear fragmentation (yellow arrows) and apoptotic bodies (green arrows). **(c)** cAgNSs-LEMF, Hep-2 cells showing shrunken apoptotic cells and nuclei (red arrow) and nuclear fragmentation (yellow arrow). Apoptotic body was detected (green arrow) and Necrotic cell debris (blue arrows). H and E, Original magnification 100X, oil.

MDA's physiological and protective significance as a signaling molecule that promotes gene expression and cell survival is summed up by its cytotoxic effect, which suppresses gene expression and encourages cell death.[65] cAgNSs and cAgNSs-LEMF significantly increase MDA levels by 22.31% and 42.73% as compared to control values, respectively. This maximum increase in MDA levels served as proof that the usage of cAgNSs-LEMF prolonged the effects of oxidative stress by enhancing lipid peroxidation. This was consistent with the LEMF's alleged ability to raise the MDA level in cases of cognitive impairment and oxidative damage.[66]

Hematoxylin and Eosin Staining of Hep-2 Cells

The microscopic observation of cAgNSs, LEMF and cAgNSs-LEMF showed morphological differences in comparison to control cells (Figure 9). Hematoxylin and eosin staining of control, Hep-2 cells showed regular cellular pleomorphic and nuclear pleomorphic cells (Figure 9a). The cells of cAgNSs group showed signs of early apoptosis as cellular and nuclear shrinkage, irregular cell membrane and peripheral condensation of chromatin. Other cells revealed late apoptotic fractures of nuclear fragmentation and apoptotic bodies. Some swollen necrotic cells with mixed euchromatin and heterochromatin and ruptured cell membrane were also detected (Figure 9b). Figure 9c displayed the cells of Hep-2 that were treated with cAgNSs-LEMF where the majority of cells exhibited several apoptotic bodies, an uneven neoplastic cell membrane, and obvious necrosis with mixed heterochromatin and euchromatin breaks in necrotic cells' cell membranes.

Conclusions

This study concluded that the exposure to a 50 mT electromagnetic field for 30 min enhanced the cytotoxicity, pro-apoptotic, and oxidant patterns of polyvinyl alcohol capped silver nanostructures against human laryngeal carcinoma Hep-2 cells. The outcomes included an approximately 6-fold increase in cytotoxicity, increased proapoptotic activity, which was demonstrated by annexin-v staining, improved mRNA expression of genes associated to apoptosis, increased levels of oxidative stress biomarkers, and hematoxylin and eosin staining.

More in vivo research is strongly urged for the therapeutic deployment of the investigated delivery system with dual benefits of silver nanostructures and extremely-low frequency Electromagnetic Field.

Author Contributions

In all phases of the study's idea, design, implementation, data collection, analysis, writing, interpretation, and final article approval, all authors made substantial contributions. Each author decided on the publication to which the article would be submitted, and they all agreed to take responsibility for every aspect of the research.

Disclosure

The authors declare no conflicts of interest.

References

1. Ma L-J, Niu R, Wu X, et al. Quantitative evaluation of cellular internalization of polymeric nanoparticles within laryngeal cancer cells and immune cells for enhanced drug delivery. *Nanoscale Res Lett*. 2021;16(1):1–14. doi:10.1186/s11671-021-03498-y
2. Wang Z, Xie W, Guan H. Diverse functions of MiR-425 in human cancer. *DNA Cell Biol*. 2023;42(3):113–129. doi:10.1089/dna.2022.0557
3. Bethesda M. Seer cancer stat facts: Female breast cancer. *Natl Cancer Inst*. 2021; 2021:1.
4. Obid R, Redlich M, Tomeh C. The treatment of laryngeal cancer. *Oral and Maxillofacial Surgery Clinics*. 2019;31(1):1–11. doi:10.1016/j.coms.2018.09.001
5. Pelaz B, Alexiou C, Alvarez-Puebla RA, et al. Diverse applications of nanomedicine. *ACS nano*. 2017;11(3):2313–2381. doi:10.1021/acsnano.6b06040
6. Shi J, Kantoff PW, Wooster R, Farokhzad OC. Cancer nanomedicine: progress, challenges and opportunities. *Nat Rev Cancer*. 2017;17(1):20–37. doi:10.1038/nrc.2016.108
7. Elveny M, Khan A, Nakhjiri AT, Albadarin AB. A state-of-The-art review on the application of various pharmaceutical nanoparticles as a promising technology in cancer treatment. *Arabian J Chem*. 2021;14(10):103352. doi:10.1016/j.arabjc.2021.103352
8. Barabadi H, Hosseini O, Damavandi Kamali K, et al. Emerging theranostic silver nanomaterials to combat lung cancer: A systematic review. *J Cluster Sci*. 2020;31:1–10. doi:10.1007/s10876-019-01639-z
9. Burdușel A-C, Gherasim O, Grumezescu AM, Mogoantă L, Ficai A, Andronescu E. Biomedical applications of silver nanoparticles: An up-to-date overview. *Nanomaterials*. 2018;8(9):681. doi:10.3390/nano8090681
10. Lin J, Huang Z, Wu H, et al. Inhibition of autophagy enhances the anticancer activity of silver nanoparticles. *Autophagy*. 2014;10(11):2006–2020. doi:10.4161/auto.36293
11. AshaRani P, Low Kah Mun G, Hande MP, Valiyaveettil S. Cytotoxicity and genotoxicity of silver nanoparticles in human cells. *ACS nano*. 2009;3(2):279–290. doi:10.1021/nn800596w
12. Foldbjerg R, Olesen P, Hougaard M, Dang DA, Hoffmann HJ, Autrup H. PVP-coated silver nanoparticles and silver ions induce reactive oxygen species, apoptosis and necrosis in THP-1 monocytes. *Toxicol Lett*. 2009;190(2):156–162. doi:10.1016/j.toxlet.2009.07.009
13. Nallathamby PD, Xu X-HN. Study of cytotoxic and therapeutic effects of stable and purified silver nanoparticles on tumor cells. *Nanoscale*. 2010;2(6):942–952. doi:10.1039/c0nr00080a
14. Sanpui P, Chattopadhyay A, Ghosh SS. Induction of apoptosis in cancer cells at low silver nanoparticle concentrations using chitosan nanocarrier. *ACS Appl Mater Interfaces*. 2011;3(2):218–228. doi:10.1021/am100840c
15. Ostad SN, Dehnad S, Nazari ZE, et al. Cytotoxic activities of silver nanoparticles and silver ions in parent and tamoxifen-resistant T47D human breast cancer cells and their combination effects with tamoxifen against resistant cells. *Avicenna j Medic Biotech*. 2010;2(4):187.
16. Meng Q, Wang A, Hua H, et al. Intranasal delivery of huperzine A to the brain using lactoferrin-conjugated N-trimethylated chitosan surface-modified PLGA nanoparticles for treatment of Alzheimer's disease. *Int j Nanomed*. 2018;13:705. doi:10.2147/IJN.S151474
17. Xu R, Ma J, Sun X, et al. Ag nanoparticles sensitize IR-induced killing of cancer cells. *Cell Res*. 2009;19(8):1031–1034. doi:10.1038/cr.2009.89
18. Gurunathan S, Lee K-J, Kalishwaralal K, Sheikpranbabu S, Vaidyanathan R, Eom SH. Antiangiogenic properties of silver nanoparticles. *Biomaterials*. 2009;30(31):6341–6350. doi:10.1016/j.biomaterials.2009.08.008
19. Liu J, Zhao Y, Guo Q, et al. TAT-modified nanosilver for combating multidrug-resistant cancer. *Biomaterials*. 2012;33(26):6155–6161. doi:10.1016/j.biomaterials.2012.05.035
20. Sriram MI, Kanth SBM, Kalishwaralal K, Gurunathan S. Antitumor activity of silver nanoparticles in Dalton's lymphoma ascites tumor model. *Int j Nanomed*. 2010;5:753–762. doi:10.2147/IJN.S11727
21. Foroozandeh P, Aziz AA. Insight into cellular uptake and intracellular trafficking of nanoparticles. *Nanoscale Res Lett*. 2018;13(1):1–12. doi:10.1186/s11671-018-2728-6
22. Alshehri MA, Wierzbicki PM, Kaboo HF, et al. In vitro evaluation of electroporated gold nanoparticles and extremely-low frequency electromagnetic field anticancer activity against Hep-2 laryngeal cancer cells. *Folia Histochemica Et Cytobiologica*. 2019;57(4):159–167. doi:10.5603/FHC.a2019.0018
23. Chen G, Upham BL, Sun W, et al. Effect of electromagnetic field exposure on chemically induced differentiation of friend erythroleukemia cells. *Environ Health Perspect*. 2000;108(10):967–972. doi:10.1289/ehp.00108967
24. Al-Humaidi RB, Fayed B, Shakartalla SB, et al. Optimum inhibition of MCF-7 breast cancer cells by efficient targeting of the macropinocytosis using optimized paclitaxel-loaded nanoparticles. *Life Sci*. 2022;305:120778. doi:10.1016/j.lfs.2022.120778
25. Girgert R, Schimming H, Körner W, Gründker C, Hanf V. Induction of tamoxifen resistance in breast cancer cells by ELF electromagnetic fields. *Biochem Biophys Res Commun*. 2005;336(4):1144–1149. doi:10.1016/j.bbrc.2005.08.243

26. Barbault A, Costa FP, Bottger B, et al. Amplitude-modulated electromagnetic fields for the treatment of cancer: discovery of tumor-specific frequencies and assessment of a novel therapeutic approach. *J Exp Clin Cancer Res*. 2009;28(1):1–10. doi:10.1186/1756-9966-28-51
27. Galloni P, Marino C. Effects of 50 Hz magnetic field exposure on tumor experimental models. *Bioelectromagnetics*. 2000;21(8):608–614. doi:10.1002/1521-186X(200012)21:8<608::AID-BEM7>3.0.CO;2-Z
28. Yasui M, Kikuchi T, Ogawa M, Otaka Y, Tsuchitani M, Iwata H. Carcinogenicity test of 50 Hz sinusoidal magnetic fields in rats. *Bioelectromagnetics*. 1997;18(8):531–540. doi:10.1002/(SICI)1521-186X(1997)18:8<531::AID-BEM1>3.0.CO;2-3
29. Abdel-Fattah WI, Ali GW. On the anti-cancer activities of silver nanoparticles. *J Appl Biotechnol Bioeng*. 2018;5(2):1–4.
30. Elbehairi SEI, Ahmed AE, Alshati AA, et al. Prosopis juliflora leave extracts induce cell death of MCF-7, HepG2, and LS-174T cancer cell lines. *EXCLI J*. 2020;19:1282. doi:10.17179/excli2020-2830
31. Bashmail HA, Alamoudi AA, Noorwali A, et al. Thymoquinone synergizes gemcitabine anti-breast cancer activity via modulating its apoptotic and autophagic activities. *Sci Rep*. 2018;8(1):11674. doi:10.1038/s41598-018-30046-z
32. Kammoun AK, Hegazy MA, Khedr A, Awan ZA, Khayat MT, Al-Sawahli MM. Etodolac fortified sodium deoxycholate stabilized zein nanoplatforms for augmented repositioning profile in human hepatocellular carcinoma: Assessment of bioaccessibility, anti-proliferation, pro-apoptosis and oxidant potentials in HepG2 cells. *Pharmaceuticals*. 2022;15(8):916. doi:10.3390/ph15080916
33. Khayat MT, Zarka MA, El-Telbany DFA, et al. Intensification of resveratrol cytotoxicity, pro-apoptosis, oxidant potentials in human colorectal carcinoma HCT-116 cells using zein nanoparticles. *Sci Rep*. 2022;12(1):15235. doi:10.1038/s41598-022-18557-2
34. Akbarnejad Z, Eskandary H, Dini L, et al. Cytotoxicity of temozolomide on human glioblastoma cells is enhanced by the concomitant exposure to an extremely low-frequency electromagnetic field (100 Hz, 100 G). *Biomed Pharmacother*. 2017;92:254–264. doi:10.1016/j.biopha.2017.05.050
35. Cameron IL, Markov MS, Hardman WE. Optimization of a therapeutic electromagnetic field (EMF) to retard breast cancer tumor growth and vascularity. *Can Cell Inter*. 2014;14(1):1–10. doi:10.1186/s12935-014-0125-5
36. Filipovic N, Djukic T, Radovic M, et al. Electromagnetic field investigation on different cancer cell lines. *Can Cell Inter*. 2014;14(1):1–10. doi:10.1186/s12935-014-0084-x
37. Tofani S, Barone D, Berardelli M, et al. Static and ELF magnetic fields enhance the in vivo anti-tumor efficacy of cis-platin against lewis lung carcinoma, but not of cyclophosphamide against B16 melanotic melanoma. *Pharmacol Res*. 2003;48(1):83–90.
38. Ronchetto F, Barone D, Cintorino M, et al. Extremely low frequency-modulated static magnetic fields to treat cancer: A pilot study on patients with advanced neoplasm to assess safety and acute toxicity. *Bioelectromagnetics*. 2004;25(8):563–571. doi:10.1002/bem.20029
39. Wang T, Nie Y, Zhao S, Han Y, Du Y, Hou Y. Involvement of midkine expression in the inhibitory effects of low-frequency magnetic fields on cancer cells. *Bioelectromagnetics*. 2011;32(6):443–452. doi:10.1002/bem.20654
40. Muthukrishnan L, Chellappa M, Nanda A, et al. Bio-fabrication of pigment-capped silver nanoparticles encountering antibiotic-resistant strains and their cytotoxic effect towards human epidermoid larynx carcinoma (HEp-2) cells. *RSC Adv*. 2019;9(28):15874–15886. doi:10.1039/C9RA01072F
41. Horie M, Fujita K. Toxicity of metal oxides nanoparticles. *Adv MolecToxic*. 2011;145–178.
42. Takechi-Haraya Y, Ohgita T, Demizu Y, Saito H, Izutsu K-I, Sakai-Kato K. Current status and challenges of analytical methods for evaluation of size and surface modification of nanoparticle-based drug formulations. *AAPS Pharm Sci Tech*. 2022;23(5):150. doi:10.1208/s12249-022-02303-y
43. Hao E, Schatz GC. Electromagnetic fields around silver nanoparticles and dimers. *The Journal of Chemical Physics*. 2004;120(1):357–366. doi:10.1063/1.1629280
44. Saliev T, Baiskhanova DM, Akhmetova A, et al. Impact of electromagnetic fields on in vitro toxicity of silver and graphene nanoparticles. *Electromagn Biol Med*. 2019;38(1):21–31. doi:10.1080/15368378.2018.1534740
45. Ghorbani P, Namvar F, Homayouni-Tabrizi M, Soltani M, Karimi E, Yaghmaei P. Apoptotic efficacy and antiproliferative potential of silver nanoparticles synthesised from aqueous extract of sumac (Rhus coriaria L.). *IET Nanobiotechnol*. 2018;12(5):600–603. doi:10.1049/iet-nbt.2017.0080
46. Chang K, Chang WH-S, Tsai M-T, Shih C. Pulsed electromagnetic fields accelerate apoptotic rate in osteoclasts. *Connective Tissue Res*. 2006;47(4):222–228. doi:10.1080/03008200600858783
47. Shinde P, Agraval H, Srivastav AK, Yadav UC, Kumar U. Physico-chemical characterization of carvacrol loaded zein nanoparticles for enhanced anticancer activity and investigation of molecular interactions between them by molecular docking. *Int J Pharm*. 2020;588:119795. doi:10.1016/j.ijpharm.2020.119795
48. Devarajan E, Sahin AA, Chen JS, et al. Down-regulation of caspase 3 in breast cancer: A possible mechanism for chemoresistance. *Oncogene*. 2002;21(57):8843–8851. doi:10.1038/sj.onc.1206044
49. Levine AJ. p53, the cellular gatekeeper for growth and division. *cell*. 1997;88(3):323–331. doi:10.1016/S0092-8674(00)81871-1
50. Fabregat I. Dysregulation of apoptosis in hepatocellular carcinoma cells. *World J Gastroenterol*. 2009;15(5):513. doi:10.3748/wjg.15.513
51. Zhu L, Guo D, Sun L, et al. Activation of autophagy by elevated reactive oxygen species rather than released silver ions promotes cytotoxicity of polyvinylpyrrolidone-coated silver nanoparticles in hematopoietic cells. *Nanoscale*. 2017;9(17):5489–5498. doi:10.1039/C6NR08188F
52. Mayo MW, Baldwin AS. The transcription factor NF-κB: Control of oncogenesis and cancer therapy resistance. *Biochimica Et Biophysica Acta (BBA)-Reviews on Cancer*. 2000;1470(2):M55–M62. doi:10.1016/S0304-419X(00)00002-0
53. Akter M, Atique Ullah A, Banik S, et al. Green synthesized silver nanoparticles-mediated cytotoxic effect in colorectal cancer cells: NF-κB signal induced apoptosis through autophagy. *Biol Trace Elem Res*. 2021;199:3272–3286. doi:10.1007/s12011-020-02463-7
54. Ghosh S, Tergaonkar V, Rothlin CV, et al. Essential role of tuberous sclerosis genes TSC1 and TSC2 in NF-κB activation and cell survival. *Cancer Cell*. 2006;10(3):215–226. doi:10.1016/j.ccr.2006.08.007
55. Pattingre S, Tassa A, Qu X, et al. Bcl-2 antiapoptotic proteins inhibit Beclin 1-dependent autophagy. *Cell*. 2005;122(6):927–939. doi:10.1016/j.cell.2005.07.002
56. Sharifi-Rad M, Anil Kumar NV, Zucca P, et al. Lifestyle, oxidative stress, and antioxidants: Back and forth in the pathophysiology of chronic diseases. *Front Physiol*. 2020;11:694. doi:10.3389/fphys.2020.00694
57. Ehnert S, Fentz A-K, Schreiner A, et al. Extremely low frequency pulsed electromagnetic fields cause antioxidative defense mechanisms in human osteoblasts via induction of• O2− and H2O2. *Sci Rep*. 2017;7(1):14544. doi:10.1038/s41598-017-14983-9
58. Falone S, Grossi MR, Cinque B, et al. Fifty hertz extremely low-frequency electromagnetic field causes changes in redox and differentiative status in neuroblastoma cells. *Int J Biochem Cell Biol*. 2007;39(11):2093–2106. doi:10.1016/j.biocel.2007.06.001

59. Martínez-Sámano J, Torres-Durán PV, Juárez-Oropeza MA, Verdugo-Díaz L. Effect of acute extremely low frequency electromagnetic field exposure on the antioxidant status and lipid levels in rat brain. *Archiv Med Res*. 2012;43(3):183–189. doi:10.1016/j.arcmed.2012.04.003
60. Marnett LJ. Oxyradicals and DNA damage. *carcinogenesis*. 2000;21(3):361–370. doi:10.1093/carcin/21.3.361
61. Küçükgüzel ŞG, Süzgün PÇ, Cantürk F, et al. Effect of etodolac hydrazone, a new compound synthesised from etodolac, on spermatozoon quality, testicular lipid peroxidation, apoptosis and spermatozoon DNA integrity. *Andrologia*. 2016;48(2):177–188. doi:10.1111/and.12429
62. Song K, Im SH, Yoon YJ, Kim HM, Lee HJ, Park GS. A 60 Hz uniform electromagnetic field promotes human cell proliferation by decreasing intracellular reactive oxygen species levels. *PLoS One*. 2018;13(7):e0199753. doi:10.1371/journal.pone.0199753
63. Cios A, Ciepielak M, Stankiewicz W, Szymański Ł. The influence of the extremely low frequency electromagnetic field on clear cell renal carcinoma. *Int J Mol Sci*. 2021;22(3):1342. doi:10.3390/ijms22031342
64. Wolf FI, Torsello A, Tedesco B, et al. 50-Hz extremely low frequency electromagnetic fields enhance cell proliferation and DNA damage: Possible involvement of a redox mechanism. *Biochimica Et Biophysica Acta (BBA)-Molecular Cell Research*. 2005;1743(1–2):120–129. doi:10.1016/j.bbamcr.2004.09.005
65. Ayala A, Muñoz MF, Argüelles S. Lipid peroxidation: production, metabolism, and signaling mechanisms of malondialdehyde and 4-hydroxy-2-nonenal. *Oxid Med Cell Longev*. 2014;2014:1–31. doi:10.1155/2014/360438
66. Duan Y, Wang Z, Zhang H, et al. The preventive effect of lotus seedpod procyanidins on cognitive impairment and oxidative damage induced by extremely low frequency electromagnetic field exposure. *Food Funct*. 2013;4(8):1252–1262. doi:10.1039/c3fo60116a